Journal of Nuclear Materials 382 (2008) 170–175

Contents lists available at ScienceDirect

Journal of Nuclear Materials

journal homepage: www.elsevier.com/locate/jnucmat

Microstructures of beta-silicon carbide after irradiation creep deformation at elevated temperatures

Yutai Katoh *, Sosuke Kondo, Lance L. Snead

Materials Science and Technology Division, Oak Ridge National Laboratory, P.O. Box 2008, Oak Ridge, TN 37830-6138, USA

A B S T R A C T

Microstructures of silicon carbide were examined by transmission electron microscopy (TEM) after creep deformation under neutron irradiation. Thin strip specimens of polycrystalline and monocrystalline, chemically vapor-deposited, beta-phase silicon carbide were irradiated in the high flux isotope reactor to 0.7–4.2 dpa at nominal temperatures of 640–1080 °C in an elastically pre-strained bend stress relaxation configuration with the initial stress of ~100 MPa. Irradiation creep caused permanent strains of 0.6 to 2.3×10^{-4}. Tensile-loaded near-surface portions of the crept specimens were examined by TEM. The main microstructural features observed were dislocation loops in all samples, and appeared similar to those observed in samples irradiated in non-stressed conditions. Slight but statistically significant anisotropy in dislocation loop microstructure was observed in one irradiation condition, and accounted for at least a fraction of the creep strain derived from the stress relaxation. The estimated total volume of loops accounted for 10–45% of the estimated total swelling. The results imply that the early irradiation creep deformation of SiC observed in this work was driven by anisotropic evolutions of extrinsic dislocation loops and matrix defects with undetectable sizes.

Published by Elsevier B.V.

1. Introduction

Beta-phase silicon carbide (SiC) is employed as a structural shell in TRISO-coated fuel system for high temperature gas-cooled reactors (HTGR) [1]. In this application, chemically vapor-deposited (CVD) dense SiC serves as a primary pressure boundary to retain high pressure due to gaseous fission products within individual tiny coated fuel particles, and as a diffusion barrier to gaseous and solid fission products. SiC was selected for its advantages such as neutron tolerance to high doses, strength retained up to very high temperatures, and chemical inertness at elevated temperatures.

Beta-phase SiC in fibrous composite forms, which is often referred to by $SiC^{(f)}$/SiC composite, is also considered for various applications in advanced energy systems. SiC/SiC composites have been studied as advanced options for blanket structures of magnetic and inertial fusion systems [2]. They are also recently considered suitable materials for insulating liners of liquid metal flow channels for certain fusion blanket types, along with other materials such as monolithic and porous SiC [3]. Moreover, SiC/SiC composites are considered promising materials for control rod sleeves of helium-cooled reactors, and a potential advanced fuel cladding material for light water reactors and gas-cooled and salt-cooled reactors [4–7]. For these applications, the benefit of using SiC/SiC composites comes primarily from the added reliability owing to fibrous reinforcement, in addition to the various advantages inherent to SiC.

Irradiation creep is an important phenomenon for materials for radiation service, because it is a major contributor to potential dimensional instability of materials under irradiation at such temperatures that thermal creep is not anticipated. Although irradiation creep often determines irradiated lifetime of metallic structural components, it is not necessarily undesirable for brittle materials like ceramics for functional applications, because it may relax and/or redistribute stresses. For SiC-based nuclear components, the latter function of irradiation creep can be very important, particularly when a significant temperature gradient exists and the secondary stresses developed by differential swelling can be severe [8].

Studies on neutron irradiation creep of SiC have so far been extremely limited and insufficient. Price published the result of the irradiation creep study on CVD SiC in 1977 [1]. In that work, elastically bent strip samples were irradiated in a fission reactor, and the linear-averaged creep compliance was estimated to be in the order of 10^{-38} [Pa n/m^2 ($E > 0.18$ MeV)]$^{-1}$, or 10^{-7} [MPa dpa]$^{-1}$, at 780–1130 °C. In a recent publication, Katoh et al. concludes that creep strains for CVD SiC were dominated by transient creep at temperatures below ~950 °C whereas steady-state creep is likely at higher temperatures with a compliance of $1.5 \pm 0.8 \times 10^{-6}$ [MPa dpa]$^{-1}$ [9]. The present work is intended to help understand the irradiation creep mechanisms in SiC, by clarifying the influence

* Corresponding author. Tel.: +1 865 576 5996; fax: +1 865 241 3650.
E-mail address: katohy@ornl.gov (Y. Katoh).

0022-3115/$ - see front matter Published by Elsevier B.V.
doi:10.1016/j.jnucmat.2008.08.012

of externally applied stress on the order of 100 MPa on microstructural development in beta-phase SiC during neutron irradiation to relatively low doses.

2. Experimental procedure

Materials used were high purity, polycrystalline CVD SiC (Rohm and Haas Co., Advanced Materials, Waborn, Massachusetts, USA) and monocrystalline 3C–SiC (Hoya Advanced Semiconductors Technologies, Inc., Tokyo, Japan). The manufacturer-claimed purity of the polycrystalline material is >99.9995%, whereas the monocrystalline wafer was n-type doped with nitrogen ($\sim 1 \times 10^{19}$ cm^{-3} carrier density) but otherwise of very high purity. Thin strip samples with dimensions of 25 mm × 1 mm × 50 μm were prepared. The monocrystalline samples were with {100} surface orientation and were machined so that the longitudinal direction was parallel with one of the <011> orientations.

In a bend stress relaxation (BSR) irradiation creep experiment, thin strip samples are elastically bent to a fixed radius during irradiation. The initial and final stresses, σ_0 and σ_a, respectively, are calculated using the measured initial (constrained) bend radius (R_0), the unconstrained residual bend radius after irradiation (R_a), specimen thickness (t) and literature values for temperature dependent elastic modulus (E)

$$\sigma_0 = \frac{Et}{2R_0}, \sigma_a = \frac{Et}{2}\left(\frac{1}{R_0} - \frac{1}{R_a}\right) \quad (1)$$

The irradiation was performed in the High Flux Isotope Reactor (HFIR) at Oak Ridge National Laboratory (Oak Ridge, Tennessee, USA) to a maximum neutron fluence of 4.2×10^{25} n/m^2 ($E > 0.1$ MeV). An equivalence of one displacement per atom (dpa) = 1×10^{25} n/m^2 ($E > 0.1$ MeV) is assumed hereafter. The nominal irradiation temperatures were 640–1080 °C. No measurable stress relaxation by thermal creep is anticipated at these temperatures for CVD-produced polycrystalline SiC [10]. Details of the irradiation technique and the result of creep strain measurement are published elsewhere [9].

Thin foil specimens for TEM examination were prepared from the tension side of the flexurally deformed samples utilizing a sectioning and back-thinning process. In this process, the tension side surface was first removed by ~1 μm to eliminate the layer which might have been affected by surface effects, followed by perforation from the compression side of the specimen. Thus, the areas for TEM examination were applied approximately 96% of the maximum flexural stress on the strip samples in an almost uni-axial tensile mode during irradiation. Argon ion beam accelerated to 3 keV were used for both processes at a milling angle of ~6°. TEM examination was performed using a Philips Tecnai 20 operated at 200 kV.

3. Results

The irradiation and stress conditions for the specimens examined by TEM are listed in Table 1, along with a summary of irradiation creep strains and microstructural features. A polycrystalline sample was examined for the irradiation condition of 640 °C/3.7 dpa, whereas monocrystalline samples were examined for the conditions of 1030 °C/0.7 dpa and 1080 °C/4.2 dpa.

After irradiation at 640 °C to 3.7 dpa, the observed microstructural defects were stacking faults and tiny spot-like clusters. For this sample, the initial and final stresses were 87 and 36 MPa, respectively. Fig. 1 presents a weak beam dark field image of the polycrystalline specimen with the beam direction B near [011] and the diffraction vector g parallel to [200]. The stacking faults were separated by 50–500 nm as typical in as-deposited CVD SiC,

Table 1
Summary of microstructural data

		CR4RH	CR7SX	CR8SX
Material		R&H CVD poly-beta SiC	Hoya monocrystalline 3C–SiC	Hoya monocrystalline 3C–SiC
T_{irr}-nominal	°C	640	1030	1080
Fluence-nominal	dpa	3.7	0.7	4.2
Initial/final stress	MPa	87/46	86/57	101/0
Creep strain		1.12×10^{-4}	0.63×10^{-4}	2.29×10^{-4}
Defects observed		Tiny loops and BSD*	Mostly Frank loops	Frank loops
Average defect diameter	nm	~3.9	~3.3	~12
Defect number density	m^{-3}	$\sim 2.8 \times 10^{23}$	$\sim 2.1 \times 10^{23}$	$\sim 3.8 \times 10^{22}$
Estimated swelling by loops		$\sim 1.1 \times 10^{-3}$	$\sim 5.1 \times 10^{-4}$	$\sim 1.4 \times 10^{-3}$
Estimated unstressed swelling		$\sim 1.1 \times 10^{-2}$	$\sim 1.5 \times 10^{-3}$	$\sim 3 \times 10^{-3}$

* Black spot defects.

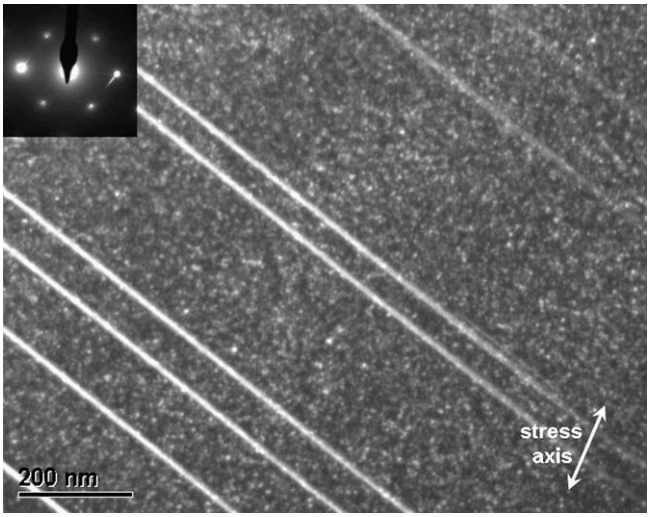

Fig. 1. Weak beam dark field image of the tensile side of chemically vapor-deposited polycrystalline SiC specimen irradiated at ~640 °C to 3.7 dpa under initial/final stress of 87/46 MPa. $B \sim [011]$, $g = [200]$, $g/4$ g. Arrow indicates the stress axis.

and are not believed to have been modified during irradiation. The spot-like clusters mostly appear as loops at higher magnifications and are presumably of the same type(s) as previously observed in CVD SiC irradiated at 800 °C [11,12]. An anisotropy analysis was not carried out for these loops, because their Burgers vectors or habit planes had not been identified.

Neutron irradiation at 1030 °C to 0.7 dpa produced tiny (typically a few nanometers in diameter) dislocation loops as the only defects observed in the monocrystalline specimen by conventional TEM. The initial stress of 86 MPa relaxed to 57 MPa at the end of irradiation for this sample. To identify characteristics of these loops, a visibility test with different diffraction vectors was performed. In Fig. 2, weak beam dark field images at an edge of the wedge (001) foil are compared in diffraction conditions [$g = \bar{2}20$] (A), $g = [040]$ (B), and $g = [220]$ (C). If loops are of Frank faulted type with Burgers vector of $a/3$<111>, then in theory, all loops should be visible using the [040] diffraction and a half of them visible in the other two conditions. Note that the visible loops using [$\bar{2}20$] and the ones visible using [220] are exclusive each other. If all clusters are perfect loops with Burgers vector of

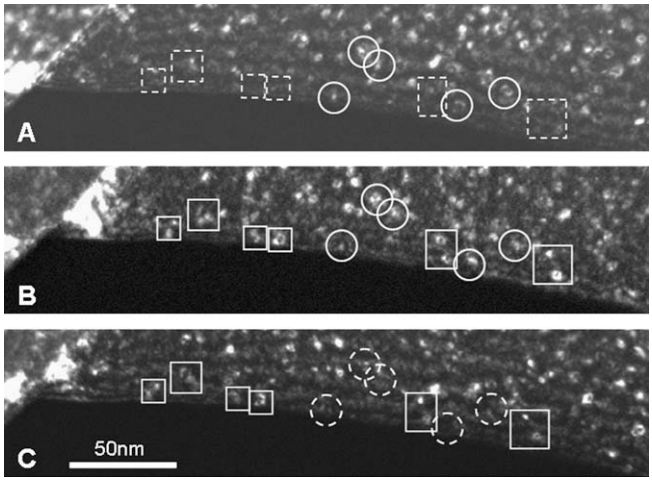

Fig. 2. Weak beam dark field images of the tensile side of chemically vapor-deposited monocrystalline SiC specimen irradiated at ~1030 °C to 0.7 dpa under initial/final stress of 86/57 MPa. Images (A)–(C) were taken from the exactly identical area with $B \sim [001]$, $g = [\bar{2}20]$, [040], and [220], respectively. Loops imaged with strong contrast are surrounded by solid symbols, whereas those with no or weak contrast are surrounded by dashed symbols.

$a/2\langle 110\rangle$, the diffraction conditions $[g = \bar{2}20]$, [040], and [220] should image 5/6, 2/3, and 5/6 of the entire loop population, respectively. Fig. 2 indicate that a substantially greater number of loops along the edge are seen with $g = [040]$ than with $g = \langle 220\rangle$. Moreover, $[g = \bar{2}20]$ and $g = [220]$ conditions image partial populations of the loops which are almost exclusive each other. Therefore, it is likely that the dislocation loops produced in this irradiation condition are mostly Frank faulted loops.

The thin foil specimen was taken from the tension side subsurface of the crept sample, as described in the previous section. In this discussion, crystallographic coordination assumes the surface normal to [001] and the stress axis parallel with [110]. Within four {111} Frank loop habit planes, $(\bar{1}11)$ and $(1\bar{1}1)$ planes are parallel with the stress axis, whereas the (111) and $(11\bar{1})$ planes intersect with it at an angle of ~35°. For convenience sake, hereafter we call the former two planes 'zero-stress' loop planes and the latter two planes 'finite-stress' loop planes.

In Fig. 3, weak beam dark field images of the 1030 °C/0.7 dpa specimen are compared for diffraction vectors $g = [220]$ (A) and $[g = 2\bar{2}0]$ (B) within the same area. The elliptical symbols drawn on Thompson tetrahedra indicate {111} planes on which the supposedly visible Frank loops are located. The arrows in white represent the axis of tensile stress applied during irradiation. Obviously, only loops on the finite-stress planes are supposedly imaged in Fig. 3(A), whereas the rest or loops on the zero-stress planes are seen in Fig. 3(B), assuming all loops are of Frank faulted type. No difference in loop number density or size between the finite-stress and zero-stress orientations could be noticed.

Frank faulted loops also were the dominant microstructural features observed in the monocrystalline specimen following neutron irradiation at 1080 °C to 4.2 dpa. The initial tensile stress of 101 MPa had completely recovered to ~0 MPa before the end of irradiation. Loop to loop interactions have already occurred at limited locations in this specimen, however, the majority of the loops remained unreacted. The loops were clearly lying on {111} planes, and the presence of intense <111> satellite streaks in selected area diffraction patterns in the absence of stacking faults (other than Frank loops) confirmed the abundance of Frank faulted loops. The streak images of edge-on loops on two different {111} planes are shown in Fig. 4. These micrographs were taken with $B \sim [011]$, and satellite streaks along $[11\bar{1}]$ (A) and $[1\bar{1}1]$ (B), as indicated by the shaded planes on the inset Thompson tetrahedra. Hence, the micrograph (A) shows Frank loops on one of the two finite-stress loop planes and the micrograph (B) shows those on one of the two zero-stress loop planes. Again, there is no significant difference in loop characteristics between the two populations.

Loop characteristics of the finite-stress and zero-stress loop planes are quantified and summarized in Table 2. For the irradiation condition of 1030 °C/0.7 dpa, loop number density appeared ~20% higher on the finite-stress loop planes than on the zero-stress planes, whereas the average loop sizes were about the same. The difference in number density is rather minor but statistically significant, considering the fact that more than 300 loops were counted in each diffraction condition from two different areas. The loop number density was higher on the finite-stress loop planes for nearly all sizes, as compared for size distribution in Fig. 5. For this irradiation condition, it should be noted that the quantification of loop sizes involves substantial uncertainty due to the small sizes and the foil drifting during the TEM image

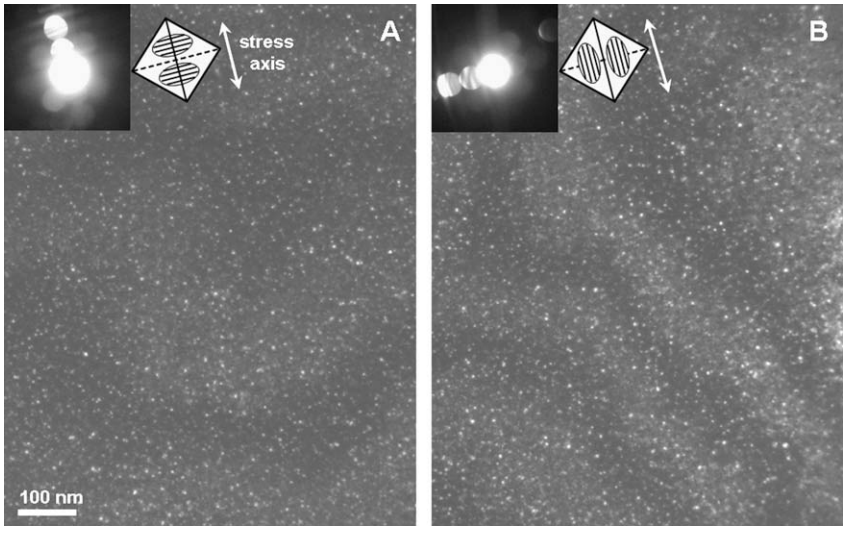

Fig. 3. Weak beam dark field images of the tensile side of chemically vapor-deposited monocrystalline SiC specimen irradiated at ~1030 °C to 0.7 dpa under initial/final stress of 86/57 MPa. Images (A) and (B) were taken from the identical area. Imaging conditions are $B \sim [001]$, $g = [220]$ (A) and $B \sim [001]$, $g = [2\bar{2}0]$ (B). Arrows indicate the stress axis [110]. Elliptical symbols shown on Thompson tetrahedra indicate loop planes imaged.

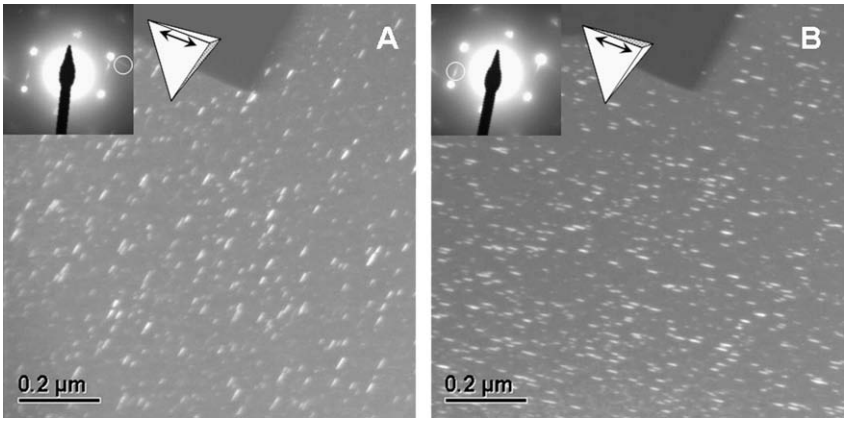

Fig. 4. Streak images of the tensile side of chemically vapor-deposited monocrystalline SiC specimen irradiated at ~1080 °C to 4.2 dpa under initial/final stress of 101/0 MPa. Images (A) and (B) were taken from the identical area. Images were from [1 1 $\bar{1}$] satellite streak (A) and from [1 $\bar{1}$ 1] satellite streak (B) at $B \sim$ [0 1 1]. Arrows and shaded planes on Thompson tetrahedra indicate the stress axis [1 1 0] and loop planes imaged, respectively.

Table 2
Comparison of loop microstructures on different loop planes

		CR7SX			CR8SX		
T_{irr}-nominal	°C	1030			1080		
Fluence-nominal	dpa	0.7			4.2		
Initial/final stress	MPa	86/57			101/0		
(Loop planes)		Finite-stress {1 1 1} planes	Zero-stress {1 1 1} planes	All {1 1 1} planes	Finite-stress {1 1 1} planes	Zero-stress {1 1 1} planes	All {1 1 1} planes
Average loop radius	nm	1.6	1.7	1.7	6.0	6.0	6.0
Defect number density	m^{-3}	1.2×10^{23}	9.7×10^{22}	2.1×10^{23}	1.8×10^{22}	1.9×10^{22}	3.8×10^{22}
Estimated swelling by loops		2.6×10^{-4}	2.5×10^{-4}	5.1×10^{-4}	7.0×10^{-4}	7.4×10^{-4}	1.4×10^{-3}
Unstressed swelling estimated from literature data				$\sim 1.5 \times 10^{-3}$			$\sim 3 \times 10^{-3}$

recording. On the other hand, for the irradiation condition of 1080 °C/4.2 dpa, loop sizes were quantified with much more confidence because most of the loops were larger than 10 nm in diameter. In this condition, both the loop number density and the average loop size appeared comparable on the finite-stress and the zero-stress loop planes within statistical uncertainties. The loop size distributions may appear slightly different but are actually about the same when smoothed.

4. Discussion

4.1. Comparison with microstructural development during unstressed irradiation

In neutron-irradiated high purity CVD SiC, it has been reported that tiny non-faulted dislocation loops dominates the microstructures at irradiation temperatures <~800 °C to a dose level of at

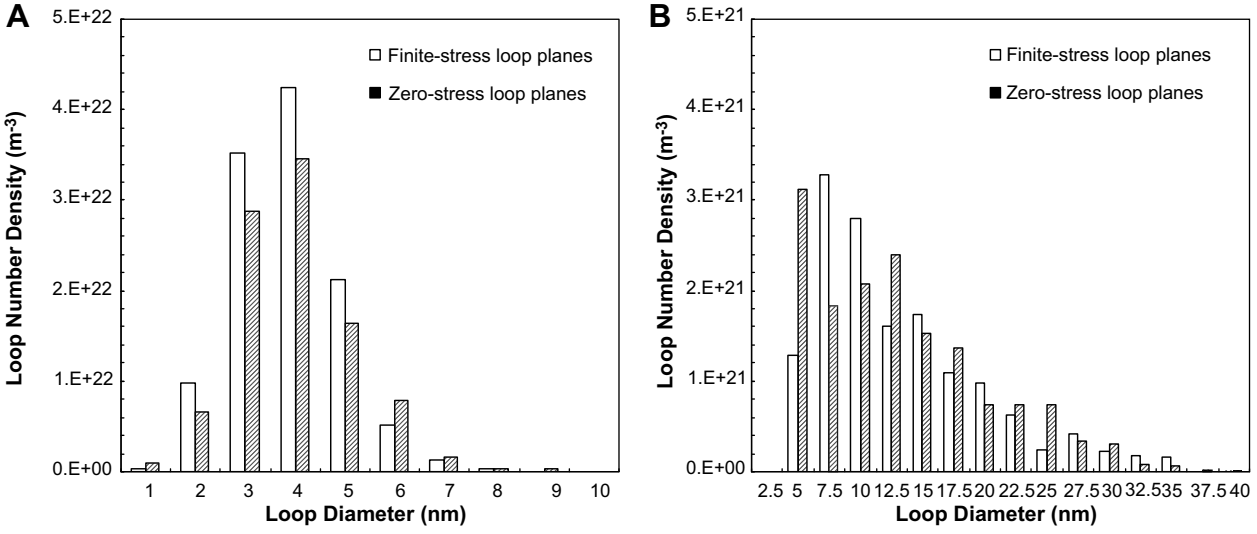

Fig. 5. Comparison of size distribution for loops with Burger's vector near-parallel and normal to tensile stress axis in chemically vapor-deposited monocrystalline SiC specimen irradiated at ~1030 °C to 0.7 dpa under initial/final stress of 86/57 MPa (A) and at ~1080 °C to 4.2 dpa under initial/final stress of 101/0 MPa (B).

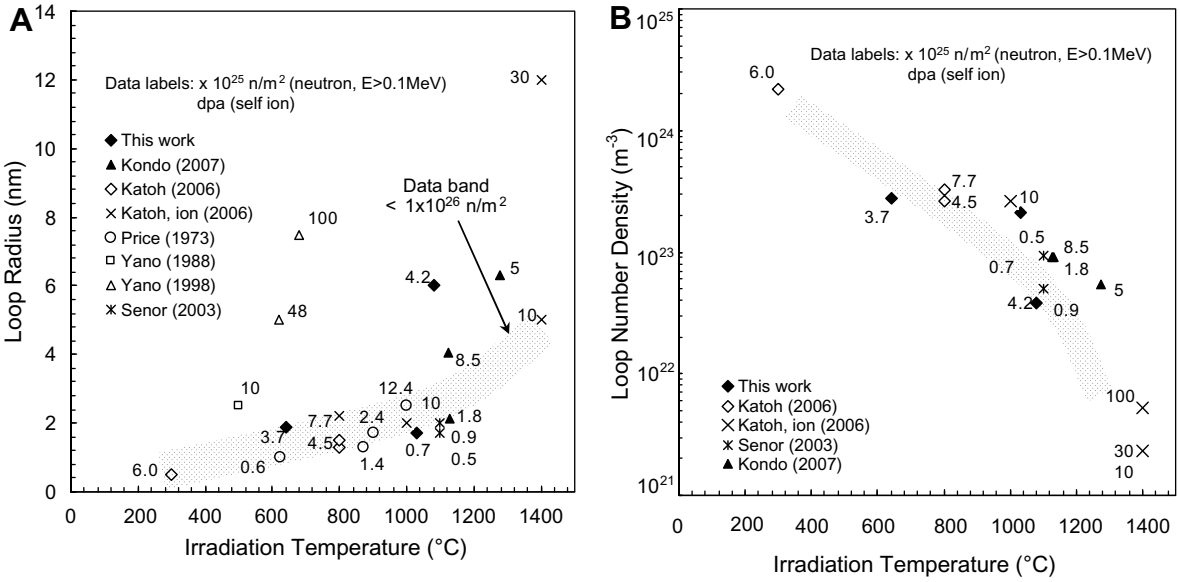

Fig. 6. Average loop radius and loop number density in chemically vapor-deposited SiC irradiated under external stresses; comparison with literature data for unstressed conditions.

least ~8 dpa [11], whereas Frank faulted loops dominates at >~1100 °C until dislocation interactions become significant [11,13,14]. There should be a transition from the non-faulted loop domination to the faulted loop domination likely between ~800 and ~1100 °C, although the lowest temperature for Frank faulted loops to develop could be even lower according to other reports [15,16]. In the present work, as shown in Figs. 1–4 and Table 1, microstructural defects which had been produced by neutron irradiation under tensile stress and were observed in conventional TEM were tiny non-faulted dislocation loops at 640 °C/3.7 dpa, tiny dislocation loops most of which are likely Frank loops at 1030 °C/0.7 dpa, and fairly well-grown Frank loops at 1080 °C/4.2 dpa. These observed microstructures were those anticipated to develop during non-stressed neutron irradiation.

In Fig. 6, average radius and number density of dislocation loops observed in the creep-deformed samples are graphically compared with the data from the non-stressed irradiation. The 640 °C/3.7 dpa and the 1030 °C/0.7 dpa data points fit in the temperature-dependence data bands for non-stressed irradiation. The 1080 °C/4.2 dpa data point for loop size significantly deviates from the data band. However, it is unlikely to have been caused by the applied stress, because the loop characteristics did not differ between planes with finite and zero-stress components. Considering the fact that the loop number density data point is located at the lower edge of the data band, the most likely reason for the rather anomalously rapid loop growth is a deviation of actual irradiation temperature from the nominal one.

4.2. Anisotropy in loop development

The above observations imply that applied stress in the magnitude range studied in this work do not impose very significant influences on the species, number density, and size of the irradiation-produced defects in SiC. On the other hand, in the 1030 °C/0.7 dpa sample, loop population on the habit plane with finite normal and shear stress components was ~20% greater than that on the plane with zero normal and shear stress components, which is statistically significant.

In ion-irradiated CVD SiC, a very significant anisotropy in the distribution of Frank loops has been reported by Kondo, et al. [17]. In their experiment, Rohm and Haas high purity CVD SiC samples were irradiated with 5.1 MeV silicon ions at 1400 °C to ~34 dpa, and it was found that number density of the Frank loops produced on individual {1 1 1} planes is clearly correlated with an angle of the loop plane relative to the irradiated surface. This anisotropy was attributed primarily to the constraint against lateral expansion due to the shallow thickness of the irradiated layer as compared to the sample thickness, in contrast to the free expansion allowed along the surface normal. Based on the present result and the Kondo work, it is likely that external stress causes an anisotropic Frank loop development. Although it is difficult to estimate the magnitude of lateral compressive stress developed during the ion irradiation, it could be significantly higher than the stress levels applied in the present work, considering that volumetric swelling of ion-irradiated SiC at 1400 °C is roughly estimated to be ~0.4% and the Young's modulus ~410 GPa [18]. The difference in extent of anisotropy between the two works may have been caused by difference in stress magnitude, irradiation temperature, dose rate, or other factors.

In the present work, anisotropy in the loop microstructure was not detected in the 1080 °C/4.2 dpa sample, although it was apparent in the sample irradiated at a slightly lower temperature and lower dose. The potential explanations for this apparent discrepancy include: (1) dislocation interactions already significant in the 1080 °C/4.2 dpa sample cancelled the stress-induced anisotropy which may had existed at lower doses (calculated mean dislocation line spacing is ~15 nm compared to ~12 nm mean loop diameter), (2) substantial neutron dose after significant stress relaxation cancelled the anisotropy (0.7 dpa at 1030 °C already relaxed 1/3 of the initial stress), and (3) stress effect is substantially different at the two temperatures (particularly the actual temperature difference may have been more significantly).

4.3. Comparison of microstructural data with macroscopic strain

In such a condition that (1) the majority of vacancies surviving mutual annihilation stay in the matrix, (2) interstitials are mobile enough and clusters only into extrinsic dislocation loops, and (3) microstructural sinks of other types are not present, the number of interstitials clustering into loops approximately equals the number of vacancies left in the matrix. In this case, macroscopic swelling should approximately correspond with the total loop volume

fraction, and if the swelling is anisotropic, the strain components decomposed along the loop normals should roughly correspond with the volume fractions of loops on individual loop planes.

However, in this work, both the measured creep strain and the unstressed volumetric swelling seem to be significantly greater than those estimated based solely on loop microstructures. In fact, for the 1030 °C/0.7 dpa condition, the strain estimated from the microstructural data normal to the loop plane with the finite-stress is only $\sim 1 \times 10^{-5}$ greater than that normal to the loop plane with zero-stress (Table 2). From the anisotropic loop microstructure data, strain along the stress axis is calculated to be $\sim 5 \times 10^{-6}$ greater than the average linear strain. Uncertainty in this estimated loop contribution to the creep strain is large because a small change in loop radius results in large change. Nevertheless, the anisotropic swelling due to anisotropic loop development likely accounts only for a fraction of the measured creep strain of 6.3×10^{-5} (Table 1). Similarly, the magnitude of swelling estimated from the microstructural data accounts for 10–45% of the swelling values typically anticipated for SiC irradiated without applied stress and in otherwise corresponding conditions (Table 1). Such substantial discrepancies of the estimated loop volume from the macroscopic swelling have been historically reported at relatively low temperatures at which vacancies are believed to be practically immobile, and attributed to the assumed presence of defect clusters which are not visible by conventional TEM techniques [11,19].

Thermal creep, particularly the primary and/or transient creep, of high purity, crystalline SiC has been studied and often attributed to grain boundary-related phenomena (such as grain boundary diffusion and grain rearrangement) and grown-in defects including stacking faults [20,21]. However, in the present work, high purity polycrystalline and monocrystalline SiC samples were irradiated in a BSR configuration side by side, and there was relatively little difference between the two materials in stress relaxation behavior. The monocrystalline sample was not only free from grain boundaries but also contained very few stacking faults or no line dislocations in a pre-irradiation condition. Both materials possess the theoretical mass density of beta-phase SiC, implying very low concentrations of grown-in vacancies.

In the monocrystalline samples, the likelihood of the migrating irradiation-produced point defects to escape to the surface is negligible, even if one does not assume the likely presence of invisible defects, because the mean dislocation inter-spacing of the visible loops alone is calculated to be <10 nm for the case of 1030 °C/0.7 dpa irradiation. Therefore, annihilation or trapping of migrating point defects are possible only at the matrix defects or clusters. In this microstructural condition, defects contributing to irradiation creep have to be matrix defects and/or clusters. Because the defects visible in TEM accounted only for limited fractions of the irradiation creep strains, the present result suggests that invisible matrix defect clusters could be the major contributors to creep. Visible loops may have played a rather supplemental role to irradiation creep (and swelling) at least for the conditions studied in this work, although the relative loop contribution may change at higher stresses or higher temperatures. The contributing invisible clusters can only be speculated and possibly are small SIA or vacancy clusters and complex clusters involving antisite defects [22].

5. Conclusions

High density non-faulted and faulted dislocation loops, respectively, were produced in high purity beta-phase CVD SiC during neutron irradiation to 3.7 dpa at ~640 °C and 0.7 or 4.2 dpa at 1030–1080 °C in a bend stress relaxation configuration with the initial stresses ~100 MPa. The dislocation loop microstructures were both qualitatively and quantitatively similar to those that typically develop under irradiation without application of external stresses.

In the monocrystalline samples, resolved stress components were zero for two of the four faulted loop planes and were finite for other two planes. Difference in loop number density between the two sets of planes was apparent only in 1030 °C/0.7 dpa condition. On the other hand, averages and distributions of loop size were not significantly different between the two sets of planes in any irradiation condition.

The estimated creep strain due to the anisotropic loop microstructure did not fully account for the measured macroscopic creep strain. Similarly, volumetric swelling values estimated from the loop microstructures accounted for less than a half of the typical macroscopic swelling values for irradiated SiC. These observations imply significant contributions to both irradiation creep and swelling from matrix defects which were not observed by TEM.

Acknowledgements

The authors would like to thank Dr Y. Matsukawa for reviewing the manuscript. The irradiation program in this research was sponsored by the US Department of Energy Office of Nuclear Energy, Science and Technology, a Nuclear Energy Research Initiative (NERI) Project, under contract NEAF355 (AF3510) with UT-Battelle, LLC. The microstructural characterization and analysis were sponsored by the US Department of Energy Office of Fusion Energy Sciences under contract DE-AC05-00OR22725 with UT-Battelle, LLC,

References

[1] R.J. Price, Nucl. Technol. 35 (1977) 320.
[2] Y. Katoh, L.L. Snead, C.H. Henager, A. Hasegawa, A. Kohyama, B. Riccardi, J.B.J. Hegeman, J. Nucl. Mater. 367–370 (2007) 659.
[3] N.B. Morley, S. Malang, I. Kirillov, Fusion Sci. Technol. 47 (2005) 488.
[4] Y. Katoh, L.L. Snead, T. Nozawa, W.E. Windes, N.B. Morley, Adv. Sci. Technol. 45 (2006) 1915.
[5] H. Feinroth, GN-54-03, Gamma Engineering, 2005.
[6] M. Konomura, T. Mizuno, T. Saigusa, Y. Ohkubo, A Promising Gas-Cooled Fast Reactor Concept and its R&D Plan, GLOBAL 2003, New Orleans, 2003.
[7] C. Forsberg, Fuel Geometry Options for Salt-Cooled Advanced High-Temperature Reactors, ICAPP 2007 Paper 7405, Nice, France, 2007.
[8] S. Smolentsev, N.B. Morley, M. Abdou, Fusion Sci. Technol. 50 (2006) 107.
[9] Y. Katoh, L.L. Snead, T. Hinoki, S. Kondo, A. Kohyama, J. Nucl. Mater. 367–370 (2007) 758.
[10] C.H. Carter Jr., R.F. Davis, J. Bentley, J. Am. Ceram. Soc. 67 (1984) 732.
[11] Y. Katoh, N. Hashimoto, S. Kondo, L.L. Snead, A. Kohyama, J. Nucl. Mater. 351 (2006) 228.
[12] S. Kondo, K.H. Park, Y. Katoh, A. Kohyama, Fusion Sci. Technol. 44 (2003) 181.
[13] D.J. Senor, G.E. Youngblood, L.R. Greenwood, D.V. Archer, D.L. Alexander, M.C. Chen, G.A. Newsome, J. Nucl. Mater. 317 (2003) 145.
[14] S. Kondo, Y. Katoh, L.L. Snead, J. Nucl. Mater. 382 (2–3) (2008) 160.
[15] R.J. Price, J. Nucl. Mater. 48 (1973) 47.
[16] T. Yano, T. Iseki, Philos. Mag. A 62 (1990) 421.
[17] S. Kondo, A. Kohyama, J. Nucl. Mater. 367–370 (2007) 764.
[18] L.L. Snead, T. Nozawa, Y. Katoh, T.S. Byun, S. Kondo, D.A. Petti, J. Nucl. Mater. 371 (2007) 329.
[19] L.L. Snead, Y. Katoh, S. Connery, J. Nucl. Mater. 367–370 (2007) 677.
[20] G.N. Morscher, J.A. DiCarlo, J. Am. Ceram. Soc. 75 (1992) 136.
[21] J.A. DiCarlo, J. Mater. Sci. 21 (1986) 217.
[22] M. Bockstedte, A. Mattausch, O. Pankratov, Phys. Rev. B 69 (2004) 235202-1.